Construction and sorption properties of pyrene-based porous aromatic frameworks

Zhuojun Yan,[a] Hao Ren,[a] Heping Ma,[a] Rongrong Yuan,[a] Ye Yuan,[a] Xiaoqin Zou, [a] Fuxing Sun[a] and Guangshan Zhu*[a,b]

[a] State Key Laboratory of Inorganic Synthesis and Preparative Chemistry, College of Chemistry, Jilin University, Changchun, 130012, China.

Fax: +86 431 85168331; Tel: +86 431 85168331; E-mail: zhugs@jlu.edu.cn

[b] Queensland Micro- and Nanotechnology Centre, Griffith University, Queensland, 4111, Australia.

Abstract

We report here pyrene-based fluorescent porous aromatic frameworks (PAF-19 and PAF-20), which are constructed by a quadrilateral building unit 1,3,6,8-tetrabromopyrene (TBrPy) with linkers 1,4-diethynylbenzene and 1,3,5-triethynylbenzene *via* Sonogashira-Hagihara coupling reaction, respectively. TG analysis shows that PAF-19 and PAF-20 are thermally stable up to 350 °C in air condition. Both materials also exhibit high chemical stability and cannot dissolve or decompose in any common organic solvents. N_2 sorption results reveal that the BET surface areas of PAF-19 and PAF-20 are 250 m^2 g^{-1} and 702 m^2 g^{-1}, respectively. They also display relatively high sorption abilities for hydrogen and carbon dioxide. H_2O sorption measurements demonstrate that the skeletons of PAF-19 and PAF-20 are highly hydrophobic. Interestingly, PAF-19 and PAF-20 exhibit excellent sorption abilities to organic chemical pollutants at the saturated vapor pressure and room temperature. PAF-20 can adsorb large amounts of methanol and benzene, with values of 609 mg g^{-1} and 1038 mg g^{-1}, respectively. The good performances of PAF-19 and PAF-20 with high sorption selectivity promise their potential application for eliminating environmental pollutants in presence of H_2O.

Keywords

1. Introduction

In recent years, many advances have been made in the design and synthesis of porous organic frameworks (POFs) with good mechanical stability, high surface area, controlled surface functionality, and their wide applications in fields of gas storage, molecular separation and catalysis, etc. [1-3] POFs prepared by elaborative selection of building blocks and connection *via* robust covalent bonds, have been classified according to different types of chemical reactions, such as base-mediated aromatic nucleophilic substitution reaction [4-9], imide formation reaction [10-15], Pd-mediated Sonogashira-Hagihara coupling reaction [16-22], Pd-mediated Suzuki coupling reaction [23-27], Ni(cod)$_2$-mediated Yamamoto coupling reaction [28-33], ZnCl$_2$ mediated nitrile cyclotrimerization reaction [34-39], borate ester formation reaction [40-43], borate anhydride formation reaction [44-47], FeCl$_3$-mediated thiophenyl-thiophenyl oxidative coupling reaction [48,49], lithium-mediated element-carbon bond formation reaction [50,51], etc. The excellent performances of POFs make themselves appropriate as gas storage media, such as H$_2$ and CH$_4$ storage and CO$_2$ capture, which are current concerns in clean energy and environment issues [52,62]. Organic chemical pollutants in air as grievous environmental problem have received unprecedented public attention. Porous materials, such as zeolites, activated carbons and inorganic-organic hybrids, have shown their abilities to deal with organic pollutants in some extent [53-56]. However, their further application has been limited by lower adsorption capacity, broad pore size distribution or low chemical stability in comparison with some reported POFs. Very recently, we have successfully synthesized a series of porous aromatic frameworks (PAFs) [26,33], revealing high adsorption capacities for organic chemical molecules such as benzene, methanol and toluene due to their aromatic networks. In this paper, we report the synthesis and characterizations of two pyrene-based fluorescent PAF materials, PAF-19 and PAF-20. As illustrated in Fig. 1, PAF-19 and PAF-20 are constructed by a quadrilateral building unit 1,3,6,8-tetrabromopyrene (TBrPy) with a linear linker 1,4-diethynylbenzene and a triangular linker 1,3,5-triethynylbenzene *via* Sonogashira-Hagihara coupling reaction, respectively. PAF-19 and PAF-20 with plentiful phenyl rings in networks exhibit permanent porosity, high thermal and chemical stabilities, and excellent sorption abilities towards organic chemical pollutants at the saturated vapor pressure and room temperature.

2. Experimental

2.1. Materials

1,3,5-Triethynylbenzene, tetrakis(triphenylphosphine)palladium and copper(I) iodide were received from Alfa Aesar. 1,4-Diethynylbenzene was received from Tokyo Kasei (TCI, 98%). *N,N*-Dimethylformamide (DMF) and triethylamine (Et$_3$N) were dried with CaH$_2$ prior to use. Other chemicals and solvents were purchased from commercial suppliers and used as received. TBrPy was prepared according to a previously reported literature [57].

2.2. Synthesis of PAF-19 and PAF-20

In the synthesis of PAF-19, TBrPy (0.5 mmol, 259 mg), 1,4-diethynylbenzene (1.5 mmol, 189 mg), tetrakis(triphenyl-phosphine)palladium (30 mg) and copper(I) iodide (10 mg) were added to a round-bottomed flask. Anhydrous DMF (5 mL) and Et$_3$N (5 mL) were added through a syringe. The reaction mixture was heated to 80 °C under N$_2$ atmosphere for 72 h. After cooling to room temperature, the crude product was filtered and washed with chloroform, methanol, and acetone to remove any unreacted monomers or catalyst residues. Further purification of the polymers was carried out by Soxhlet extraction with tetrahydrofuran for 48 h. The product was dried in vacuum for 24 h at 60 °C to give PAF-19 (197 mg). PAF-20 was synthesized using the similar procedure with a replacement of 1,4-diethynylbenzene by 1,3,5-triethynylbenzene (1.0 mmol, 150 mg). Around 188 mg of the final PAF-20 product was obtained after washing and drying.

2.3. Characterizations

The FTIR spectra were collected on an IFS 66V/S Fourier transform infrared spectrometer using KBr pellets. The thermalgravimetric analysis (TGA) was performed using a TA model TGA Q500 thermal analyzer system up to 800 ℃ under air atmosphere at a heating rate of 5 ℃ min^{-1}. Solid-state ^{13}C CP/MAS NMR measurement was carried out on a Bruker Avance III model 400 MHz NMR spectrometer at a MAS rate of 5 kHz. The SEM pictures were taken on a JEOL model JSM-6700F scanning electron microscope and Iridium (IXRF Systems) software with an accelerating voltage of 5 kV. High resolution transmission electron microscopy (HRTEM) was performed on a JEOL JEM 3010 with an acceleration voltage of 300 kV. PXRD was performed by a Riguku D/MAX2550 diffractometer using Cu-Kα radiation, 40 kV, 200 mA with a 2θ range of 4°–40°. N$_2$ and H$_2$ adsorption isotherms were measured on Quantachrome model Autosorb-1C analyzer. CO$_2$ and organic molecules sorption isotherms were measured using Autosorb iQ$_2$ (Quantachrome) adsorption analyzer.

3. Results and Discussion

3.1. Structure Characterizations

3.1.1. FTIR spectroscopy

The structures of PAF-19 and PAF-20 are firstly studied by FTIR spectroscopy. Fig. 2 shows IR spectra of initial monomers and final products. By comparison, it can be found that the characteristic absorption peak for C-Br at 495 cm^{-1} disappears, which gives an indication for the breakage of the C-Br bonds of TBrPy. In addition, the intense absorption peak associated with alkynyl C-H stretching vibration near 3300 cm^{-1} from the terminal alkyne groups vanishes. Meanwhile, a peak with low intensity is observed near 2200 cm^{-1} in the final product, which is assigned to the alkyne -C≡C- stretching vibration mode. The evidences in the IR results prove that the PAF-19 and PAF-20 are formed by the cross-coupling reaction.

3.1.2. ^{13}C CP/MAS NMR

To further reveal the local structures of PAF-19 and PAF-20 networks, solid-state ^{13}C CP/MAS NMR was performed. As shown in Fig. S1, all of the carbon signals with a chemical shift in the range of 120–140 ppm are observed, which are related to aromatic carbon atoms of building phenylene groups in the framework. Additionally, the structures with triple-bond linkages have been confirmed by the characteristic resonance of a triple-bonded carbon with a corresponding peak at around 90 ppm. The results of ^{13}C CP/MAS NMR suggest that this cross-coupling reaction is effective in the synthesis of conjugated organic polymers.

3.1.3. Powder X-ray diffraction

Powder X-ray diffraction (PXRD) was used to investigate the crystallinity of PAF-19 and PAF-20 samples (Fig. S2). It indicates that their textures are amorphous. The long-range disorder of structures could be due to the twisting between pyrene units and linkers in the networks (Fig. S3) [58,59].

3.1.4. Scanning electron microscopy and Transmission electron microscopy

Scanning electron microscopy (SEM) images (Fig. S4) show that PAF-19 and PAF-20 afforded a spherical morphology with 50–100 nm in size. High resolution transmission electron microscopy (HRTEM) images (Fig. 3) also indicate that the textures of PAF-19 and PAF-20 are amorphous but with uniform pores.

3.2. Physicochemical Properties

3.2.1. Optical properties

As clearly seen, the colors of PAF-19 and PAF-20 powders are red and yellow, respectively (Fig. S5). Further, UV-Visible spectra (Fig. S6) were collected on PAF-19, PAF-20 and TBrPy monomer. As shown in Fig. S6, both PAF-19 and PAF-20 samples show broad absorptions in the spectra, indicating their high conjugated nature. Meanwhile, the photoluminescent properties of PAF-19 and PAF-20 were also investigated using fluorescence spectroscopy by dispersing their solid samples in ethanol solvent (1.5 mg/10 ml) at room temperature (Fig. S7). The photoluminescent spectrum of PAF-19 (Fig. S7a) shows a strong emission band centered at 639 nm, and the spectrum of PAF-20 (Fig. S7b) shows a broad emission profile with three main peaks centered at 543, 585 and 623 nm, respectively. These observations are consistent with UV data.

3.2.2. Stability of PAF-19 and PAF-20

The thermal and chemical stabilities of PAF-19 and PAF-20 were investigated. As displayed in thermogravimetric analysis (TGA) curve (Fig. 4), PAF-19 and PAF-20 decompose up to 350 °C in air condition, indicating they possess high thermal stability. The chemical stability was tested by additional experiments using organic solvents (e.g. THF, acetone, ethanol, DMF, DMSO, etc.) and aqueous solution of acids and bases (1 M HCl and 1 M NaOH). It has been found that both solids cannot dissolve or decompose in these common solvents and solutions, indicating their high chemical stability.

3.2.3. N_2 sorption measurements

To characterize the porosities of the PAF-19 and PAF-20 networks, the nitrogen sorption isotherms were measured on the activated samples at 77 K from 0 to 1 bar. As shown in Fig. 5a, the N_2 sorption isotherm of PAF-19 displays a typical microporous feature of a high uptake at the low relative pressure, followed by a steady increase at the high relative pressure. Similarly, an analogous isotherm is observed in PAF-20 sample (Fig. 5b). To be mentioned, PAF-20 exhibits an exceptionally high N_2 uptake of 1215 $cm^3 \cdot g^{-1}$ at $P/P_0 = 0.99$. When the Brunauer–Emmett–Teller (BET) model is adopted to calculate the apparent surface area, the surface areas of PAF-19 and PAF-20 are 250 $m^2 \cdot g^{-1}$ and 702 $m^2 \cdot g^{-1}$, respectively. Although the surface areas are not very high among reported POFs, these values still exceed some well-studied micro- and mesoporous materials [60,61]. Derived from appropriate non-local density functional theory (NL-DFT) model, PAF-19 and PAF-20 exhibit narrow pore-size distributions with mean pore sizes of 1.33 nm and

1.38 nm, respectively. Estimated from the amount of gas uptake at $P/P_0 = 0.99$ (Fig. S8), the total pore volume is 0.43 cm^3 g^{-1} and 1.88 cm^3 g^{-1} for PAF-19 and PAF-20 respectively, while the cumulative pore volume derived from NL-DFT is 0.28 cm^3 g^{-1} (PAF-19) and 1.45 cm^3 g^{-1} (PAF-20).

3.3. Sorption properties of PAF-19 and PAF-20

3.3.1. H₂ sorption

As well known, the porous materials are good candidates for gas sorption or storage. Based on the consideration of clean energy and environment issues, the gas sorption capacities of PAF-19 and PAF-20 are exemplified by hydrogen and carbon dioxide gases. As shown in Fig. 6a, at 1 bar, the H_2 uptake of PAF-19 is 62 $cm^3 \cdot g^{-1}$ at 77 K and 52 $cm^3 \cdot g^{-1}$ at 87 K, respectively. In the case of PAF-20 (Fig. 6a), at 1 bar, the H_2 uptake is 100 $cm^3 \cdot g^{-1}$ at 77 K and 59 $cm^3 \cdot g^{-1}$ at 87 K, respectively. The H_2 uptakes of PAF-19 and PAF-20 are comparatively lower than other POFs, but the plentiful phenyl rings in the PAF networks could lead to an enhancement for the adsorption enthalpies of H_2 (Q_{stH2}). Fig. 6b shows that PAF-19 and PAF-20 materials have Q_{st} values of 6.99 $kJ \cdot mol^{-1}$ and 8.07 $kJ \cdot mol^{-1}$ at zero loading, respectively (Details of Q_{st} calculation in Supporting Information, Fig. S9 and S10). From the Q_{stH2} list of similar materials in Table 1, the Q_{stH2} of PAF-20 is higher than most of POFs, with an exception of CMP-0–5 (~10 $kJ \cdot mol^{-1}$) [21]. Inspired by this experimental result, more efforts are still underway for the successful design of novel PAF materials with high Q_{stH2}.

3.3.2. CO₂ sorption

Encouraged by the high Q_{stH2} of PAF-19 and PAF-20, we have an enthusiasm to investigate the Q_{stCO2} of PAF-19 and PAF-20. As shown in Fig. 7a, at 1 bar, the volumetric CO_2 uptake of PAF-19 is 20.1 $cm^3 \cdot g^{-1}$ at 273 K and 13.3 $cm^3 \cdot g^{-1}$ at 298 K, respectively. For the PAF-20 sample (Fig. 7a), at 1 bar, the CO_2 uptake is 25.9 $cm^3 \cdot g^{-1}$ at 273 K and 14.7 $cm^3 \cdot g^{-1}$ at 298 K, respectively. From the adsorption isotherms of CO_2 at 273 K and 298 K (Fig. S11 and S12), the Q_{stCO2} of PAF-19 and PAF-20 are calculated to be 28.5 and 30.3 $kJ \cdot mol^{-1}$ at zero coverage, respectively (Fig. 7b). As expected, PAF-19 and PAF-20 show high Q_{stCO2} owing to their specific networks, which offer a possible arena to enhance their interactions with CO_2 molecules. It is worth mentioning that the Q_{stCO2} of PAF-20 is still ranked in a high level among the reported porous materials (Table 1).

3.3.3. Liquid sorption

Liquid sorption is becoming more and more important, especially for the removal of volatile organic compounds. In this respect, the sorption measurements of organic chemical molecules and water in PAF-19 and PAF-20 have been carried out at 298 K (Fig. 8). From the H_2O sorption isotherms, PAF-19 and PAF-20 are verified as excellent hydrophobic materials featured by small H_2O uptakes at 298 K. However, PAF-19 and PAF-20 can adsorb large amounts of methanol and benzene at the same condition. As shown in Fig. 8, steady increases in the uptakes are observed with increasing methanol or benzene vapour pressure for PAF-19 and PAF-20 samples. At the saturated vapour pressure, the sorption of methanol and benzene on PAF-19 and PAF-20 still does not reach the plateau. The adsorbed amounts of methanol and benzene on PAF-19 at 298 K are 318 mg·g^{-1} (9.9 mmol·g^{-1}) and 375 mg·g^{-1} (4.8 mmol·g^{-1}), respectively. Due to the higher BET surface area, there is no doubt that PAF-20 is able to adsorb more methanol and benzene than that of PAF-19 at 298 K, with values of 609 mg·g^{-1} (19.0 mmol·g^{-1}) and 1038 mg·g^{-1} (13.3 mmol·g^{-1}), respectively. From another table of liquid sorption list of some porous materials (Table 2), the methanol and benzene sorption abilities of PAF-19 and PAF-20 are higher than those porous materials with similar surface areas, especially for benzene adsorption. This result reveals that there are strong guest–host interactions between benzene molecules and the frameworks of PAF-19 and PAF-20, which could be ascribed to π-π interactions. The liquid sorption experiments reveal that PAF-19 and PAF-20 are highly hydrophobic materials and featured in a favorable sorption of methanol and benzene compared with H_2O. Such high selectivity towards organic compounds promises PAF-19 and PAF-20 as suitable adsorbents to eliminate harmful organic pollutants from H_2O.

4. Conclusions

We present here pyrene-based fluorescent porous aromatic frameworks, PAF-19 and PAF-20, which are constructed by a quadrilateral building unit TBrPy with respective linkers 1,4-diethynylbenzene and 1,3,5-triethynylbenzene *via* Sonogashira-Hagihara coupling reaction. PAF-19 and PAF-20 possess excellent thermal and chemical stabilities, and comparably high adsorption abilities for hydrogen and carbon dioxide. The plentiful phenyl rings in the polymer networks lead to an enhancement of the adsorption enthalpies for H_2 and CO_2. Significantly, PAF-19 and PAF-20 are highly hydrophobic materials with high methanol and benzene uptakes at

the saturated vapour pressure and room temperature. The good performances of PAF-19 and PAF-20 with high sorption selectivity make themselves as ideal candidates in the removal of environmental harmful pollutants from water.

Appendix A. Supplementary data

Supplementary data associated with this article can be found in the online version.

Acknowledgments

References

[1] N. B. McKeown, P. M. Budd, Macromolecules 43 (2010) 5163–5176.

[2] J. R. Holst, A. I. Cooper, Adv. Mater. 22 (2010) 5212–5216.

[3] R. Dawson, A. I. Cooper, D. J. Adams, Prog. Polym. Sci. 37 (2012) 530–563.

[4] P. M. Budd, B. S. Ghanem, S. Makhseed, N. B. McKeown, K. J. Msayib, C. E. Tattershall, Chem. Commun. (2004) 230–231.

[5] P. M. Budd, E. S. Elabas, B. S. Ghanem, S. Makhseed, N. B. McKeown, K. J. Msayib, C. E. Tattershall, D. Wang, Adv. Mater. 16 (2004) 456–459.

[6] B. S. Ghanem, N. B. McKeown, P. M. Budd, D. Fritsch, Macromolecules 41 (2008) 1640–1646.

[7] M. Carta, K. J. Msayib, N. B. McKeown, Tetrahedron. Lett. 50 (2009) 5954–5957.

[8] N. B. McKeown, B. Ghanem, K. J. Msayib, P. M. Budd, C. E. Tattershall, K. Mahmood, S. Tan, D. Book, H. W. Langmi, A. Walton, Angew. Chem. Int. Ed. 45 (2006) 1804–1807.

[9] B. Ghanem, N. B. McKeown, K. D. M. Harris, Z. Pan, P. M. Budd, A. Butler, J. Selbie, D. Book, A. Walton, Chem. Commun. (2007) 67–69.

[10] N. Ritter, M. Antonietti, A. Thomas, I. Senkovska, S. Kaskel, J. Weber, Macromolecules 42 (2009) 8017–8020.

[11] B. S. Ghanem, N. B. McKeown, P. M. Budd, N. M. Al-Harbi, D. Fritsch, K. Heinrich, L. Starannikova, A. Tokarev, Y. Yampolskii, Macromolecules 42 (2009) 7881–7888.

[12] J. Weber, M. Antonietti, A. Thomas, Macromolecules 41 (2008) 2880–2885.

[13]   O. K. Farha, A. M. Spokoyny, B. G. Hauser, Y. S. Bae, S. E. Brown, R. Q. Snurr, C. A. Mirkin, J. T. Hupp, Chem. Mater. 21 (2009) 3033–3035.

[14]   Z. G. Wang, B. F. Zhang, H. Lu, L. X. Sun, C. L. Jiao, W. S. Liu, Chem. Commun. (2010) 7730–7732.

[15]   O. K. Farha, Y. S. Bae, A. M. Spokoyny, B. G. Hauser, R. Q. Snurr, C. A. Mirkin, J. T. Hupp, Chem. Commun. (2010) 1056–1058.

[16]   J. X. Jiang, F. Su, A. Trewin, C. D. Wood, N. L. Campbell, H. Niu, C. Dickinson, A. Y. Ganin, M. J. Rosseinsky, Y. Z. Khimyak, A. I. Cooper, Angew. Chem. Int. Ed. 46 (2007) 8574–8578.

[17]   R. Dawson, A. Laybourn, R. Clowes, Y. Z. Khimyak, D. J. Adams, A. I. Cooper, Macromolecules 42 (2009) 8809–8816.

[18]   J. X. Jiang, F. Su, H. Niu, C. D. Wood, N. L.Campbell, Y. Z. Khimyak, A. I. Cooper, Chem. Commun. (2008) 486–488.

[19]   E. Stockel, X. F. Wu, A. Trewin, C. D. Wood, R. Clowes, N. L. Campbell, J. T. A. Jones, Y. Z. Khimyak, D. J. Adams, A. I. Cooper, Chem. Commun. (2009) 212–214.

[20]   R. Dawson, A. Laybourn, Y. Z. Khimyak, D. J. Adams, A. I. Cooper, Macromolecules 43 (2010) 8524–8530.

[21]   J. Jiang, F. Su, A. Trewin, C. D. Wood, N. L. Campbell, H. Niu, C. Dickinson, A. Y. Ganin, M. J. Rosseinsky, Y. Z. Khimyak, A. I. Cooper, J. Am. Chem. Soc. 130 (2008) 7710–7720.

[22]   J. Jiang, A. Laybourn, R. Clowes, Y. Z. Khimyak, J. Bacsa, S. J. Higgins, D. J. Adams, A. I. Cooper, Macromolecules 43 (2010) 7577–7582.

[23]   L. Chen, Y. Yang, D. Jiang, J. Am. Chem. Soc. 132 (2010) 9138–9143.

[24]   J. Weber, A. Thomas, J. Am. Chem. Soc. 130 (2008) 6334–6335.

[25]   L. Chen, Y. Hongsho, S. Seki, D. Jiang, J. Am. Chem. Soc. 132 (2010) 6742–6748.

[26]   Y. Yuan, F. X. Sun, H. Ren, X. F. Jing, W. Wang, H. P. Ma, H. J. Zhao, G. S. Zhu, J. Mater. Chem. 21 (2011) 13498–13502.

[27]   M. Rose, N. Klein, W. Böhlmann, B. Böhringer, S. Fichtner, S. Kaskel, Soft Matter. 6 (2010) 3918–3923.

[28]   J. Schmidt, M. Werner, A. Thomas, Macromolecules 42 (2009) 4426–4429.

[29]   W. Lu, D. Yuan, D. Zhao, C. Schilling, O. Plietzsch, T. Muller, S. Brase, J. Guenther, J. Blümel, R. Krishna, Z. Li, H.-C. Zhou, Chem. Mater. 22 (2010) 5964–5972.

[30]   J. R. Holst, E. Stöckel, D. J. Adams, A. I. Cooper, Macromolecules 43 (2010) 8531–8538.

[31]   A. Trewin, A. I. Cooper, Angew. Chem. Int. Ed. 49 (2010) 1533–1535.

[32]   T. Ben, H. Ren, S. Q. Ma, D. P. Cao, J. H. Lan, X. F. Jing, W. C. Wang, J. Xu, F. Deng, J. M. Simmons, S. L. Qiu, G. S. Zhu, Angew. Chem., Int. Ed. 48 (2009) 9457–9460.

[33]   H. Ren, T. Ben, F. X. Sun, M. Y. Guo, X. F. Jing, H. P. Ma, K. Cai, S. L. Qiu, G. S. Zhu, J. Mater. Chem. 21 (2011) 10348–10353.

[34]   P. Kuhn, M. Antonietti, A. Thomas, Angew. Chem. Int. Ed. 47 (2008) 3450–3453.

[35]   P. Kuhn, A. Forget, D. Su, A. Thomas, M. Antonietti, J. Am. Chem. Soc. 130 (2008) 13333–13337.

[36]   P. Kuhn, A. Thomas, M. Antoniietti, Macromolecules 42 (2009) 319–326.

[37]   M. J. Bojddys, J. Jeromenok, A. Thomas, M. Antonietti, Adv. Mater. 22 (2010) 2202–2205.

[38]   M. J. Bojdys, S. A. Wohlgemuch, A. Thomas, M. Antonietti, Macromolecules 43 (2010) 6639–6645.

[39]   W. Zhang, C. Li, Y. P. Yuan, L. G. Qiu, A. J. Xie, Y. H. Shen, J. F. Zhu, J. Mater. Chem. 20 (2010) 6413–6415.

[40]   A. P. Cote, H. M. El-Kaderi, H. Furukawa, J. R. Hunt, O. M. Yaghi, J. Am. Chem. Soc. 129 (2007) 12914–12915.

[41]   M. Dogru, A. Sonnauer, A. Gavryushin, P. Knochel, T. Bein, Chem. Commun. (2010) 2462–2464.

[42]   S. Wang, J. Guo, J. Kim, H. Ihee, D. Jiang, Angew. Chem. Int. Ed. 47 (2008) 8826–8829.

[43]   R. W. Tilford, S. J. Mugavero, P. J. Pellechia, J. J. Lavigne, Adv. Mater. 20 (2008) 2741–2746.

[44]   A. P. Cote, A. I. Benin, N. W. Ockwig, M. O'Keeffe, A. J. Matzger, O. M. Yaghi, Science 310 (2005) 1166–1170.

[45]   H. M. El-Kaderi, J. R. Hunt, J. L. Mendoza-Cortes, A. P. Cote, R. E. Taylor, M. O'Keeffe, O. M. Yaghi, Science 316 (2007) 268–272.

[46]   F. J. Uribe-Romo, J. R. Hunt, H. Furukawa, C. Klock, M. O'Keeffe, O. M. Yaghi, J. Am. Chem. Soc. 131 (2009) 4570–4571.

[47]   H. Furukawa, O. M. Yaghi, J. Am. Chem. Soc. 131 (2009) 8875–8883.

[48]   J. Schmidt, J. Weber, J. Epping, M. Antonietti, A. Thomas, Adv. Mater. 21 (2009) 702–705.

[49]   S. W.Yuan, S. Kirklin, B. Dorney, D. J. Liu, L. P. Yu, Macromolecules 42 (2009) 1554–1559.

[50] M. Rose, W. Böhlmann, M. Sabo, S. Kaskel, Chem. Commun. (2008) 2462–2464.

[51] J. Fritsch, M. Rose, P. Wollmann, W. Böhlmann, S. Kaskel, Materials 3 (2010) 2447–2462.

[52] D. S. Zhang, Z. Chang, Y. B. Lv, T. L. Hu, X. H. Bu, RSC Adv. 2 (2012) 408–410.

[53] J. Y. Ying, C. P. Mehnert, M. S. Wong, Angew. Chem., Int. Ed. 38 (1999) 56–77.

[54] Q. H. Hu, S. Z. Qiao, F. Haghseresht, M. A. Wilson, G. Q. Lu, Ind. Eng. Chem. Res. 45 (2006) 733–738.

[55] A. B. Fuertes, G. Marban, D. M. Nevskaia, Carbon 41 (2003) 87–96.

[56] X. Q. Zou, J. E. Fallah, J. M. Goupil, G. S. Zhu, V. Valtchev, S. Mintova, RSC Adv. 2 (2012) 3115–3122.

[57] C. Venkataramana, S. Sankararaman, Eur. J. Org. Chem. 19 (2005) 4162–4166.

[58] J. X. Jiang, A. Trewin, D. J. Adams, A. I. Cooper, Chem. Sci. 2 (2011) 1777–1781.

[59] K. V. Rao, S. Mohapatra, T. K. Maji, S. J. George, Chem. Eur. J. 18 (2012) 4505–4509.

[60] K. L. Mulfort, T. M. Wilson, M. R. Wasielewski, J. T. Hupp, Langmuir 25 (2009) 503–508.

[61] F. Svec, J. Germain, J. M. J. Frechet, Small 5 (2009) 1098–1111.

[62] T. Ben, C. Y. Pei, D. L. Zhang, J. Xu, F. Deng, X. F. Jinga, S. L. Qiu, Energy Environ. Sci. 4 (2011) 3991–3999.

[63] K. B. Lee, M. G. Beaver, H. S. Caram, S. Sircar, Ind. Eng. Chem. Res. 47 (2008) 8048–8062.

[64] D. Yuan, W. Lu, D. Zhao, H.-C. Zhou, Adv. Mater. 23 (2011) 3723–3725.

[65] C. F. Martin, E. Stöckel, R. Clowes, D. J. Adams, A. I. Cooper, J. J. Pis, F. Rubiera, C. Pevida, J. Mater. Chem. 21 (2011) 5475–5483.

[66] R. Dawson, E. Stöckel, J. R. Holst, D. J. Adams, A. I. Cooper, Energy Environ. Sci. 4 (2011) 4239–4245.

[67] R. Dawson, D. J. Adams, A. I. Cooper, Chem. Sci. 2 (2011) 1173–1177.

[68] H. Li, M. Eddaoudi, M. O'Keeffe, O. M. Yaghi, Nature 402 (1999) 276–279.

[69] L. Hou, Y. Y. Lin, X. M. Chen, Inorg. Chem. 47 (2008) 1346–1351.

[70] D. X. Xue, Y. Y. Lin, X. N. Cheng, X. M. Chen, Cryst. Growth Des. 7 (2007) 1332–1336.

[71] X. Lin, A. J. Blake, C. Wilson, X. Z. Sun, N. R. Champness, M. W. George, P. Hubberstey, R. Mokaya, M. Schroder, J. Am. Chem. Soc. 128 (2006) 10745–10753.

[72] Y. Peng, T. Ben, J. Xu, M. Xue, X. F. Jing, F. Deng, S. L. Qiu, G. S. Zhu, Dalton Trans. 40 (2011) 2720–2724.

Figure Captions:

Table 1 Summary of surface areas and adsorption enthalpies (Q_{stH2}/Q_{stCO2}) for PAF-19, PAF-20 and other representative porous materials.
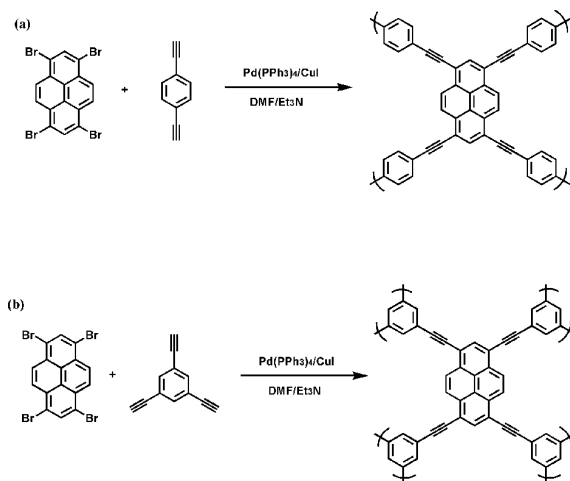
Table 2 Summary of surface areas and liquid vapour sorption (H_2O/methanol/benzene) for PAF-19, PAF-20 and other representative porous materials.

Fig. 1 Schematic illustration for the synthesis of PAF-19 (a) and PAF-20 (b).

Fig. 2 FTIR spectra of PAF-19 (a, black) and PAF-20 (b, black) polymer networks, and their respective starting materials, 1,3,6,8-tetrabromopyrene (red), 1,4-diethynylbenzene (blue), and 1,3,5-triethynylbenzene (green) in the range of 400-4000 cm^{-1}.

Fig. 3 HRTEM images of PAF-19 (a, b) and PAF-20 (c, d) samples.

Fig. 4 TGA plots for PAF-19 (black) and PAF-20 (red) polymer networks in air condition with a heating rate of 5 °C min^{-1}.

Fig. 5 Nitrogen adsorption (filled symbols)–desorption (empty symbols) isotherms for PAF-19 (a) and PAF-20 (b). The insets show the pore size distribution derived from N_2 adsorption calculated by the NL-DFT method.

Fig. 6 (a) Hydrogen adsorption (filled symbols) and desorption (empty symbols) isotherms of PAF-19 (black circle at 77 K, black triangle at 87 K), and PAF-20 (red circle at 77 K, red triangle at 87 K); (b) isosteric heats of adsorption of PAF-19 (black) and PAF-20 (red) for hydrogen.

Fig. 7 (a) Carbon dioxide adsorption (filled symbols) and desorption (empty symbols) isotherms of PAF-19 (black circle at 273 K, black triangle at 298 K), and PAF-20 (red circle at 273 K, red triangle at 298 K); (b) isosteric heats of adsorption of PAF-19 (black) and PAF-20 (red) for carbon dioxide.

Fig. 8 Water (black), methanol (blue) and benzene (red) adsorption isotherms at 298 K for PAF-19 (a) and PAF-20 (b).

Table 1 Summary of surface areas and adsorption enthalpies (Q_{stH2}/Qst_{CO2}) for PAF-19, PAF-20 and other representative porous materials.

Material	S_{BET} ($m^2 \cdot g^{-1}$)	H_2 uptake (wt %)	Q_{stH2} ($kJ \cdot mol^{-1}$)	CO_2 uptake (mmol/g)	Qst_{CO2} ($kJ \cdot mol^{-1}$)	Ref
PAF-1	5600	1.66[a]	5.4	2.05[f]	15.6	[62]
PAF-3	2932	2.07[a]	6.6	3.48[f]	19.2	[62]
PAF-4	2246	1.50[a]	6.3	2.41[f]	16.2	[62]
PAF-19	250	0.55[a]	6.99	0.90[e]	28.5	This work
PAF-20	702	0.89[a]	8.07	1.16[e]	30.3	This work
COF-1	750	1.46[b]	6.2			[47]
COF-5	1670	3.54[b]	6.0			[47]
COF-6	750	2.23[b]	7.0			[47]
COF-8	1350	3.46[b]	6.3			[47]
COF-10	1760	3.88[b]	6.6			[47]
COF-102	3620	7.16[b]	3.9			[47]
COF-103	3530	6.98[b]	4.4			[47]
PPN-1	1249	1.37[a]	7.59	11[g]	~27.5	[29]
PPN-2	1764	1.51[a]	6.89	19[g]	~22.5	[29]
PPN-3	2840	1.58[a]	5.51	25.3[g]	~18.6	[29]
PPN-4	6461	8.34[c]	4.0			[64]
HCP 1	1646			3.01[e]	23.5	[65]
HCP 2	1684			3.30[e]	21.2	[65]
HCP 3	1531			3.24[e]	22.1	[65]
HCP 4	1642			3.92[e]	21.6	[65]
MOP A	4077			2.65[e]	~24.0	[66]
MOP B	1847			3.29[e]	~22.0	[66]
MOP C	1237			3.86[e]	~34.0	[66]
MOP D	1213			2.42[e]	~26.5	[66]
MOP E	1470			2.95[e]	~25.5	[66]
MOP F	653			1.80[e]	~27.0	[66]
MOP G	1056			2.15[e]	~26.8	[66]
CMP-1	837	1.14[d]	~10.0	2.05[e]	~27.0	[21,67]
CMP-1-(OH)$_2$	1043			1.80[e]	~27.6	[67]
CMP-1-(CH$_3$)$_2$	899			1.64[e]	~26.8	[67]
CMP-1-NH$_2$	710			1.64[e]	~29.5	[67]
CMP-1-COOH	522			1.60[e]	32.6	[67]
BPL carbon	1250	1.52[b]	8.0	2.09[e]	24.3	[47,63]

[a] At 77 K and 1 bar. [b] At 77 K and saturation. [c] At 77 K and 55 bar. [d] At 77 K and 1.13 bar. [e] At 273 K and 1 bar. [f] At 273 K and 1 atm. [g] At 295 K and 60 bar.

Table 2 Summary of surface areas and liquid vapour sorption (H$_2$O/methanol/benzene) for PAF-19, PAF-20 and other representative porous materials.
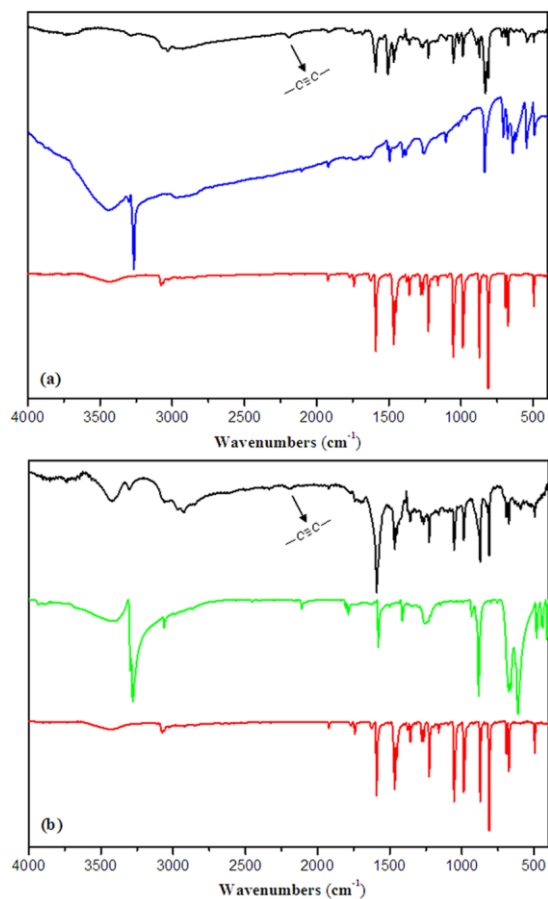
Material	S$_{BET}$ (m^2·g^{-1})	H$_2$O (mg·g^{-1})	Methanol (mg·g^{-1})	Benzene (mg·g^{-1})	T (K)	Ref
MOF-5	2900[a]			802	295	[68]
PAF-5	1503		934	917	298	[33]
[Zn$_4$O(bdc)(bpz)$_2$]·4DMF·6H$_2$O	1476		~500[c]	~620[c]	298	[69]
PAF-11	704	35	654	874	298	[26]
PAF-20	702	65	609	1038	298	[b]
[Cu$_2$(bdc)$_2$(dmf)]H$_2$O·(dmf)(C$_2$H$_5$OH)$_{0.5}$	374		~170[c]	~70[c]	298	[70]
[Zn$_2$(L)]$_\infty$	313	154	84	90	298	[71]
JUC-Z1	283	~22		273	298	[72]
PAF-19	250	26	318	375	298	[b]

[a] Langmuir surface area calculated form assuming a monolayer coverage of N$_2$. [b] This work. [c] Measured at P/P$_0$=0.9.

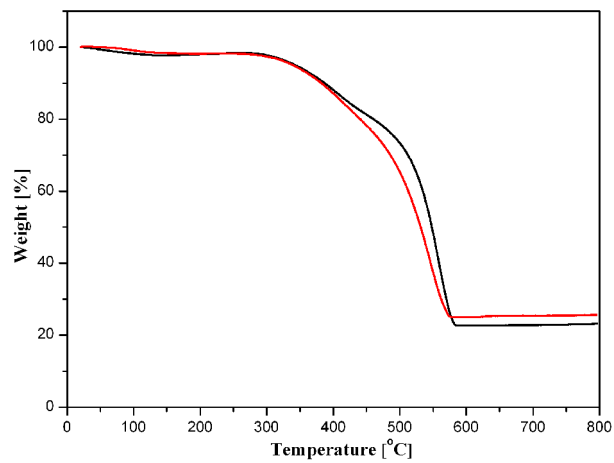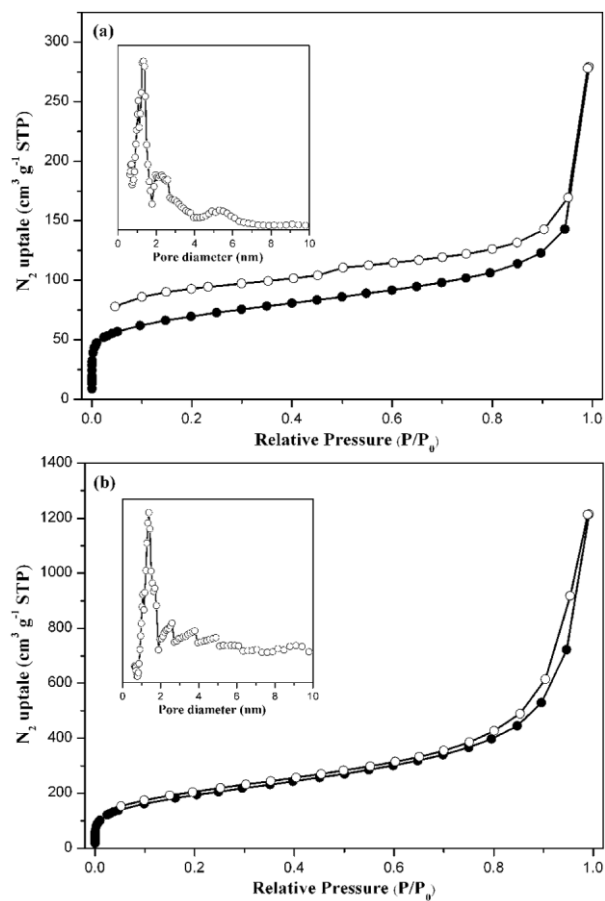**Fig. 1** Schematic illustration for the synthesis of PAF-19 (a) and PAF-20 (b).

Fig. 2 FTIR spectra of PAF-19 (a, black) and PAF-20 (b, black) polymer networks, and their respective starting materials, 1,3,6,8-tetrabromopyrene (red), 1,4-diethynylbenzene (blue), and 1,3,5-triethynylbenzene (green) in the range of 400-4000 cm^{-1}.
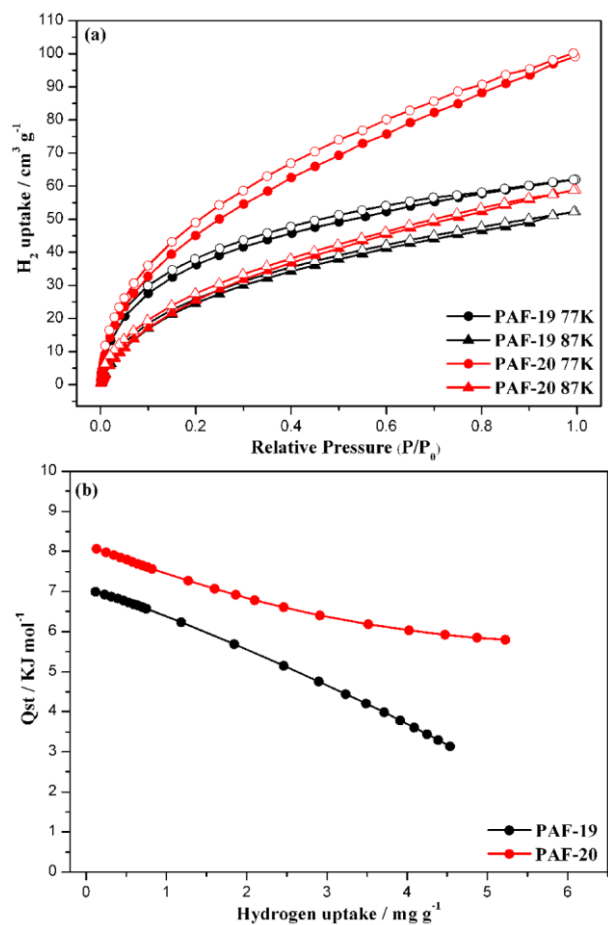
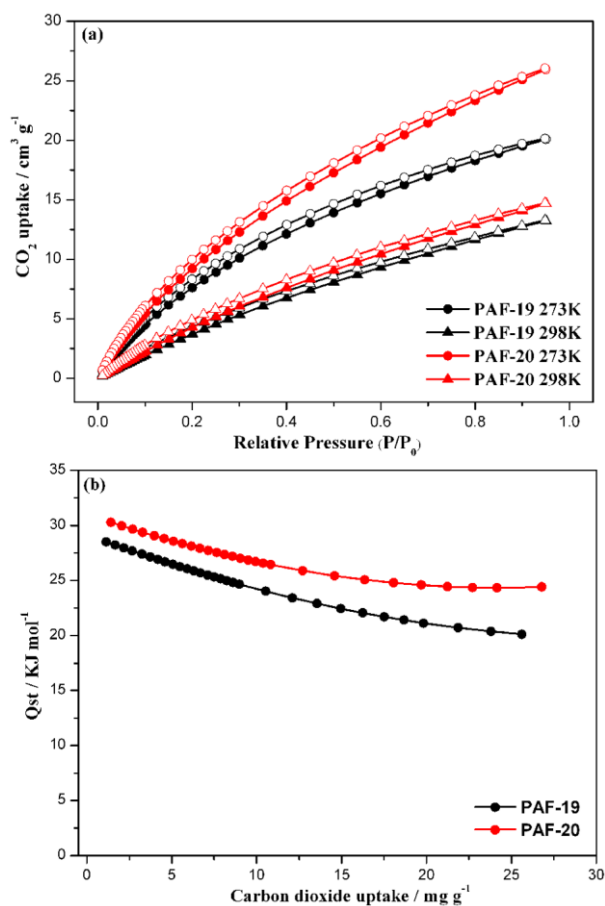**Fig. 3** HRTEM images of PAF-19 (a, b) and PAF-20 (c, d) samples.

Fig. 4 TGA plots for PAF-19 (black) and PAF-20 (red) polymer networks in air condition with a heating rate of 5 °C min^{-1}.
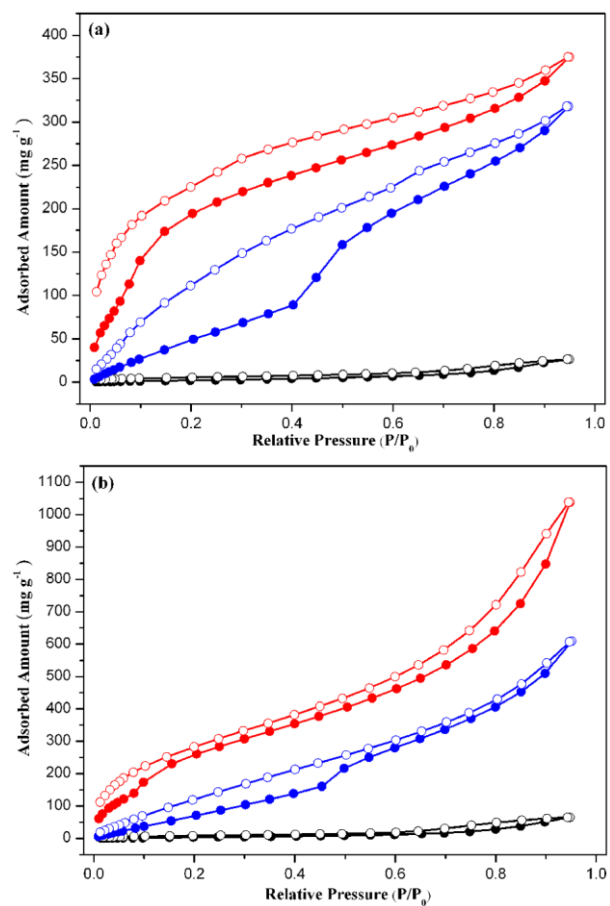
Fig. 5 Nitrogen adsorption (filled symbols)–desorption (empty symbols) isotherms for PAF-19 (a) and PAF-20 (b). The insets show the pore size distribution derived from N_2 adsorption calculated by the NL-DFT method.

Fig. 6 (a) Hydrogen adsorption (filled symbols) and desorption (empty symbols) isotherms of PAF-19 (black circle at 77 K, black triangle at 87 K), and PAF-20 (red circle at 77 K, red triangle at 87 K); (b) isosteric heats of adsorption of PAF-19 (black) and PAF-20 (red) for hydrogen.

Fig. 7 (a) Carbon dioxide adsorption (filled symbols) and desorption (empty symbols) isotherms of PAF-19 (black circle at 273 K, black triangle at 298 K), and PAF-20 (red circle at 273 K, red triangle at 298 K); (b) isosteric heats of adsorption of PAF-19 (black) and PAF-20 (red) for carbon dioxide.

Fig. 8 Water (black), methanol (blue) and benzene (red) adsorption isotherms at 298 K for PAF-19 (a) and PAF-20 (b).

Graphical abstract
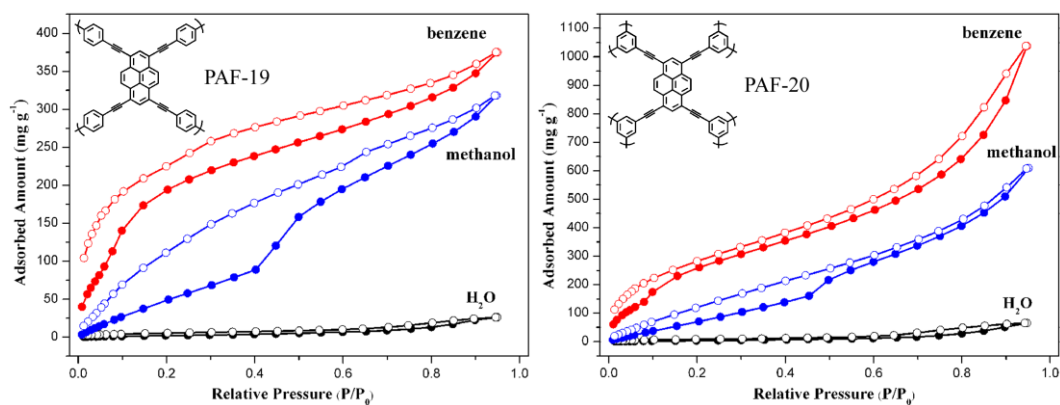
Targeted synthesis of pyrene-based porous aromatic frameworks has been achieved *via* Sonogashira-Hagihara coupling reaction. PAF-19 and PAF-20 are highly hydrophobic materials with high methanol and benzene uptakes at the saturated vapour pressure and room temperature.

Highlights

► Pyrene-based porous aromatic frameworks are synthesized *via* Sonogashira-Hagihara coupling reaction.

► The plentiful phenyl rings in the networks lead to an enhancement for the adsorption enthalpies of H_2 and CO_2.

► Materials with hydrophobic skeletons for highly selective sorption of benzene and methanol.